Published in final edited form as:
J Biomech Eng. 2010 July ; 132(7): 071008. doi:10.1115/1.4001030.

Validation of the Cat as a Model for the Human Lumbar Spine During Simulated High-Velocity, Low-Amplitude Spinal Manipulation

Allyson Ianuzzi,
Department of Biomedical Engineering, Stony Brook University, Stony Brook, NY 11794

Joel G. Pickar, and
Palmer Center for Chiropractic Research, Palmer College of Chiropractic, Davenport, IA 52803

Partap S. Khalsa
Department of Biomedical Engineering, Stony Brook University, Stony Brook, NY 11794

Allyson Ianuzzi: allyson_ianuzzi@yahoo.com

Abstract

High-velocity, low-amplitude spinal manipulation (HVLA-SM) is an efficacious treatment for low back pain, although the physiological mechanisms underlying its effects remain elusive. The lumbar facet joint capsule (FJC) is innervated with mechanically sensitive neurons and it has been theorized that the neurophysiological benefits of HVLA-SM are partially induced by stimulation of FJC neurons. Biomechanical aspects of this theory have been investigated in humans while neurophysiological aspects have been investigated using cat models. The purpose of this study was to determine the relationship between human and cat lumbar spines during HVLA-SM. Cat lumbar spine specimens were mechanically tested, using a displacement-controlled apparatus, during simulated HVLA-SM applied at L5, L6, and L7 that produced preload forces of ~25% bodyweight for 0.5 s and peak forces that rose to 50–100% bodyweight within ~125 ms, similar to that delivered clinically. Joint kinematics and FJC strain were measured optically. Human FJC strain and kinematics data were taken from a prior study. Regression models were established for FJC strain magnitudes as functions of factors species, manipulation site, and interactions thereof. During simulated HVLA-SM, joint kinematics in cat spines were greater in magnitude compared with humans. Similar to human spines, site-specific HVLA-SM produced regional cat FJC strains at distant motion segments. Joint motions and FJC strain magnitudes for cat spines were larger than those for human spine specimens. Regression relationships demonstrated that species, HVLA-SM site, and interactions thereof were significantly and moderately well correlated for HVLA-SM that generated tensile strain in the FJC. The relationships established in the current study can be used in future neurophysiological studies conducted in cats to extrapolate how human FJC afferents might respond to HVLA-SM. The data from the current study warrant further investigation into the clinical relevance of site targeted HVLA-SM.

Keywords

feline; biomechanics; low back pain; mechanical; range of motion; zygapophyseal joint; facet joint

Correspondence to: Allyson Ianuzzi, allyson_ianuzzi@yahoo.com.

1 Introduction

Lumbar spinal manipulation (SM) is an intervention utilized by physicians (primarily chiropractors and osteopaths) typically for treating patients with low back pain. Although SM is used less often than conventional therapy, twice as many patients treated with SM report that it is “very helpful” compared with conventional treatment [1]. The meta-analyses of randomized clinical trials indicate that SM is an efficacious treatment for nondiscogenic low back pain with rare incidence of serious adverse effects [2,3]. However, SM techniques have evolved empirically and the physiological mechanisms for their mode of action are only beginning to be understood [4].

High-velocity, low-amplitude (HVLA)-SM is a technique commonly employed by chiropractors, who provide the great majority (>75%) of SM treatments to patients [5]. In the lumbar spine, it has been investigated from biomechanical [6–8] and neurophysiological [9,10] perspectives. Biomechanically, HVLA-SM is characterized by a preload phase (~100 N for ~1 s) and a subsequent impulse phase (~50– 400 N for ~250 ms) [4,8]. This loading actuates the involved vertebra within the limits of its range of motion [4] and stretches the respective paraspinal joint capsules, ligaments, and muscles. Neurophysiologically, these tissues are innervated by low-threshold, mechanically sensitive neurons [11–13] and are likely stimulated by the manipulation [9,10]. Stimulation of these mechanically sensitive afferents is theorized to be an initiating mechanism for the SM’s clinical benefit in reducing low back pain [14].

The biomechanics of HVLA-SM have been studied in human spines [6–8] and combined neurophysiological and biomechanical studies [9,10] have been conducted using cat models. However, extrapolating neurophysiological data from cats to humans is not straightforward due to anatomical and physiological differences between these species. A solution to this challenge is to determine whether the biomechanics of cat and human spines during HVLA-SM can be related mathematically, as has previously been accomplished during physiological motions [15]. Because lumbar facet joint capsules (FJCs) are innervated [16–18], and mechanically stretched during HVLA-SM [6,7] with their resulting strains directly related to global lumbar spinal motion [19], lumbar FJC strain was a reasonable variable by which to determine a potential relationship. Therefore, the purpose of the current study was to establish a mathematical (i.e., regression) relationship for cat and human spines, during simulated HVLA-SM, based on FJC strains caused by the manipulation-induced vertebral kinematics. The data from simulated HVLA-SM in a cat model are reported in the current study, and data for simulated HVLA-SM in human spine specimens were taken from a previously published study [6]. It was hypothesized that a generalized linear model could be used to describe human and cat lumbar FJC strain magnitudes as a function of manipulation site, species, joint motion, and their interactions.

2 Methods

2.1 Specimen Preparation

The same cat lumbar spine specimens that were used in a prior study [15] were tested in the current study during simulated HVLA-SM. Briefly, laboratory bred cats (n = 6; mass=4.1 ± 0.1 kg; male) were obtained and their lumbar spines (L2—sacrum; cats have seven lumbar vertebrae) isolated using methods that were in accordance with the Stony Brook University Institutional Animal Care and Use Committee and the Panel on Euthanasia of the American Veterinary Medical Association. Specimens were dissected under low magnification (ten times) to remove all superficial skin, fascia, and muscle, resulting in “osteoligamentous” spine specimens. Care was taken to remove all tissue from the FJC surface such that the capsular ligament was not damaged. Specimens were potted at the sacrum using a quick-

setting epoxy (Bondo™) such that the vertebral end-plates were parallel to the testing surface.

To enable FJC strain and vertebral kinematics measurements, the specimens were prepared as follows. Imaging of the L5–6, L6–7 and L7-S1 FJC surfaces was facilitated by affixing black markers to the surfaces of the capsules. A small amount of silicon carbide particles also was dusted on the surface of each FJC to create a stochastic pattern when illuminated with a fiber optic light. Three infrared reflective markers were attached in a noncollinear fashion to each transverse process at L5, L6, and L7.

2.2 Experimental Setup

The apparatus to simulate HVLA-SM (Fig. 1) was identical to that used to simulate HVLA-SM using human cadaveric spine specimens [6]. Briefly, the experimental setup consisted of a mechanical testing apparatus, a camera system consisting of two complementary metal-oxide-semiconductor (CMOS) cameras to measure FJC strain in three dimensions (MotionPro 500, Redlake, San Diego, CA), and a commercial kinematic system for tracking vertebral kinematics (Qualysis MotionPro cameras and Track Manager System; Innovision Systems, Inc., MI; see Fig. 1). The two camera systems were calibrated before placing the cat spine specimen in the testing apparatus. The specimens were attached to a testing plate at the potted sacrum (Fig. 1 top). The most cephalic vertebra (L2) was coupled to a linear actuator (Model 317, Galil, Inc., CA) placed in-series with a force transducer (Model LCF300; Futek, CA, Range ± 110 N). No buckling of the spine or soft tissues was observed. Once positioned in its neutral posture, the L5, L6, or L7 vertebral body was coupled to a linear actuator placed in series with a force transducer. A U-shaped aluminum coupling was attached to the vertebra using an aluminum rod that went through the arms of the “U” and the anterior vertebral body. Washers with set screws were used to prevent the rod from slipping relative to the vertebra or coupling. This differed from the coupling used in the human study [6], where a Synthes Small Fragment Locking Compression Plate (Synthes, USA, Paoli, PA) had been attached to the anterior aspect of the vertebral body (L3, L4, or L5) because the size of the cat vertebral body was too small to be plated. In both studies, the coupling was attached to the motor via a swivel-head joint that had 30 degrees-of-freedom.

2.3 Mechanical Testing (HVLA-SM)

Spinal manipulation was applied at the anterior aspect of either L5, L6, or L7 through the U-shaped coupling under displacement control. The linear actuator was displaced in the *x*-direction (along the transverse axis, see Fig. 1), simultaneously creating translation and rotation of the vertebrae. Similar to the prior study using human spine specimens, the loading paradigm consisted of a preload phase (to simulate positioning of the joint near the limits of its range of motion) and a peak impulse (to simulate the impulse force administered during HVLA-SM) [8]. The displacement profile (Fig. 2) consisted of 8.5 mm total displacement. For preload, the motor displaced 2/3 of the total displacement (5.67 mm) at 10 mm/s and was then held for 500 ms. The peak impulse consisted of the remaining 1/3 displacement (2.83 mm) at 45 mm/s after which the motor returned to the starting position at 45 mm/s. These magnitudes and displacement rates were determined in preliminary studies as those which reliably produced preload force ~25% bodyweight and peak forces between 50% and 100% bodyweight [19] for programmed SM durations of 250 ms similar to the duration reported during in vivo human SM [8]. Because the mean mass of the cats was 4.1 kg, this corresponded to 10 N preload and 20–40 N peak force.

2.4 Data Analysis

Developed load was measured by the force transducer. Vertebral kinematics and left and right FJC strain magnitudes were measured optically as described in a prior study [6].

Intervertebral angle (IVA) was calculated from the three-dimensional displacements of the markers on the transverse processes. For each trial IVA was computed using the method of Soderkvist and Wedin [20], where IVA at L5–6 and L6–7 was calculated for the cephalic vertebra relative to the immediately caudal vertebra comprising that joint. At L7-S1, it was assumed that the sacrum was fixed. The relative vertebral translations (RVTs) of *x*-, *y*-, and *z*-axes, as well as total RVT (which was the vector sum of the three axis translations) were computed similarly (Fig. 2).

Plane strain of the FJC was computed using images from the two CMOS cameras, which enabled accounting for out-of-plane FJC motions during spine actuation. Images were analyzed using a custom program (MATLAB). Briefly, the black markers affixed to the FJC surface defined a plane comprising the FJC surface. For the first image (image *i*) taken by each CMOS camera, this two-dimensional plane was divided into a 3 × 3 array of subregions. Using computer-aided speckle interferometry [21], the two-dimensional displacements of these subregions were determined between subsequent images (image *i* versus image *i* + 1, image *i* + 1 versus image *i* + 2, etc.) from each camera. Principles of photogrammetry [22] were applied to calculate the three-dimensional displacements from the two 2D displacements of the FJC subregions. The 3D subregion displacements were subsequently used to compute plane strain (ε_{xx}, ε_{yy}, ε_{xy}) and principal strain ($E1$ and $E2$) as previously described [6]. As has been done in prior studies of cervical [23] and lumbar [6,7,19] FJC strain, principal strains were organized and reported as maximum (tensile) and minimum (compressive) principal strain ($\widehat{E_1}$ and $\widehat{E_2}$, respectively).

Peak strain ($\widehat{E_1}$ and $\widehat{E_2}$), IVA, and load (force or moment) for a given trial were computed as the mean peak value for the last five cycles comprising that trial, where load had reached equilibrium. L5–6, L6–7, and L7-S1 joint moments were computed as the product of the applied peak load and the moment arm (i.e., distance between the point of force application and the center of the FJC for that joint).

2.5 Statistics and Regression Relationships

One-way analysis of variance (ANOVA) was conducted to investigate whether the developed load magnitude at the initiation of preload and at peak displacement was related to the site at which HVLA-SM was delivered (L5, L6, or L7). One-way ANOVA was also utilized to determine whether RVT or IVA varied significantly with manipulation site. Two-way ANOVA was utilized to assess whether manipulation site, side of the spine or interactions thereof had a significant effect on principal strain at a given joint level. Post-hoc Tukey tests were utilized for all post-hoc analyses.

The data from a prior study in our laboratory using human spine specimens [6] were used to develop regression relationships between cat and human FJC strain magnitudes during simulated HVLA-SM. Although vertebral kinematics were reported in that study as absolute vertebral motions (i.e., they were not joint motions), relative vertebral motions were computed from the data and are presented here. Also, specimens in a prior study were actuated at different rates (5 mm/s, 20 mm/s, and 50 mm/s). Because manipulation rate did not have a significant effect on FJC strain magnitudes in a prior study, regression relationships were established using the speed for the human spine specimens (in Ref. [6], 50 mm/s) that was closest to the speed used for cat spine specimens in the present study (45 mm/s).

Regression relationships were developed for principal strain during HVLA-SM using a generalized linear model. The following general linear model was used to predict $\widehat{E_1}$ at a given joint capsule (e.g., left side cephalic joint).

$$\widehat{E_1} = c_0 + c_1 Sp + \mathrm{Loc}_1 + \mathrm{Loc}_2 Sp$$

where c_0 was a constant, Sp was a dummy variable defining species, and c_1, Loc_1, and Loc_2 were unique coefficients associated with the HVLA-SM site. JMP software (SAS, Cary NC, version 6.0.0) and $\alpha = 0.05$ were used for all statistical tests.

3 Results

3.1 Developed Load at the Manipulation Site

Loads that developed under displacement control were close in magnitude to the desired preload (10 N) and peak impulse load (20–40 N; see Fig. 3). During the preload phase under constant displacement, the load developed at the manipulated vertebra did not differ significantly with manipulation site (ANOVA; $p = 0.563$). At peak impulse, the developed load varied significantly with manipulation site (ANOVA; $p = 0.028$), where load was greater when the manipulation was applied at L7 compared with L5 or L6 (Tukey test; $p < 0.05$).

Relative vertebral translations (RVT) at segmental levels relative to the manipulation site during simulated HVLA-SM are depicted in Fig. 4 (left column). At the cephalic joint (L5–6), cat *z*-axis (right-left), *y*-axis (cranial-caudal) RVT, and total RVT were significantly greater in absolute magnitude when the manipulation was applied to the middle vertebra (L6) compared with either the cephalic (L5) or caudal (L7) vertebrae ($p < 0.05$). At the middle joint (L6–7), *y*-axis RVT was significantly greater in absolute magnitude when the HVLA-SM was applied to the caudal vertebra compared with the cephalic or middle vertebrae ($p < 0.05$). At the caudal joint (L7-S1; Fig. 4, bottom left), *x*-axis RVT was significantly greater in absolute magnitude when the HVLA-SM was applied to the caudal vertebra compared with the cephalic vertebra ($p < 0.05$).

Human RVT magnitudes during simulated HVLA-SM are depicted in Fig. 4 (right column). At the cephalic joint (L3–4), greater *x*-axis and total RVT developed when the HVLA-SM was applied to the middle joint versus the cephalic or caudal joints ($p < 0.05$). At the middle (L4–5) and caudal (L5-S1) joints, no significant association was detected between RVT and HVLA-SM site ($p < 0.05$).

3.2 IVA

Cat IVA during HVLA-SM are depicted in Fig. 5 (left column). At the cephalic joint (L5–6), *x*-axis and *z*-axis IVA was greater in absolute magnitude when the HVLA-SM was applied to the middle joint compared with the cephalic (L5) or caudal (L7) joints ($p < 0.05$). Cat cephalic joint (L5–6) total IVA also varied significantly with HVLA-SM site (in increasing order: middle [L6]>cephalic [L5]>caudal [L7]; $p < 0.05$). At the middle joint (L6–7), cat IVA about the *x*-axis was significantly greater when the HVLA-SM was applied to the caudal vertebra compared with the cephalic vertebra ($p < 0.05$). Cat L6–7 *y*-axis IVA was significantly different when the HVLA-SM was applied to the caudal vertebra compared with the cephalic or middle vertebrae, where IVA was different in direction (and hence sign; $p < 0.05$). Similarly, cat L7-S1 IVA about the *z*-axis was significantly different in direction (and sign) when the HVLA-SM was applied to the caudal vertebra compared with the cephalic vertebra ($p < 0.05$). Total IVA at L6–7 was significantly greater when the HVLA-SM was applied to the caudal vertebra compared with the middle or cephalic vertebrae ($p < 0.05$). At the caudal joint (L7-S1), cat *y*-axis IVA was significantly greater when the HVLA-SM was applied to the caudal vertebra compared with the middle or cephalic vertebrae ($p < 0.05$).

Human IVA magnitudes during simulated HVLA-SM are depicted in Fig. 5 (right column). At the cephalic joint (L4–5), *y*-axis IVA was significantly greater in absolute magnitude when the HVLA-SM was applied to the middle vertebra compared with the cephalic vertebra ($p < 0.05$). When the HVLA-SM was applied to the middle vertebra, significantly different *y*-axis IVA occurred at the middle joint (L6–7) compared with when the HVLA-SM was applied to the cephalic or caudal vertebrae. At the caudal joint (L5-S1), human *y*-axis IVA were significantly greater in magnitude when the HVLA-SM was applied to the caudal vertebra compared with the cephalic vertebra ($p < 0.05$).

3.3 FJC Maximum Principal Strain- $\widehat{E_1}$

During simulated HVLA-SM, the regional cat $\widehat{E_1}$ FJC strain magnitudes varied with the site of manipulation (Fig. 6; top). The effects of manipulation site and side of the spine on cat $\widehat{E_1}$ FJC strain magnitude depended on what joint level was considered (i.e., L5–6, L6–7, or L7-S1), as described below. Human FJC strain magnitudes from a prior study are also shown in Fig. 6 (bottom).

Cephalic joint $\widehat{E_1}$ FJC principal strain magnitudes were significantly affected by manipulation site, side of the spine and interactions thereof (two-way ANOVA; $p < 0.0010$). When the HVLA-SM was applied to the L5 (cephalic) or L6 (middle) vertebra, L5–6 FJC $\widehat{E_1}$ strain magnitudes on the left side of the spine were greater than those that developed on the right side of the spine (post-hoc Tukey test, $p < 0.05$). When the HVLA-SM was applied to the L7 (caudal) vertebra, no significant difference was detected in L5–6 FJC $\widehat{E_1}$ strain magnitudes between the left and right sides of the spine (post-hoc Tukey test, $p > 0.05$, power 70%). On the left side of the spine, L5–6 FJC $\widehat{E_1}$ strain magnitudes were significantly larger when the HVLA-SM was applied to the L6 vertebra compared with the L7 vertebra (post-hoc Tukey test, $p < 0.05$).

Cat L6–7 $\widehat{E_1}$ FJC strain magnitudes were also significantly affected by interactions between manipulation site and side of the spine (two-way ANOVA; $p = 0.04$). When the HVLA-SM was applied to the L5 vertebra, L6–7 FJC $\widehat{E_1}$ strain magnitudes were smaller compared with those that developed when the HVLA-SM was applied to the L7 vertebra (post-hoc Tukey test, $p < 0.05$). No significant differences in L6–7 FJC $\widehat{E_1}$ strain magnitudes were detected on the left or right sides of the spine (post-hoc Tukey test, $p > 0.05$, power 58%).

At L7-S1, cat FJC $\widehat{E_1}$ strain magnitudes were significantly affected by interactions between manipulation site and side of the spine (two-way ANOVA, $p = 0.02$). L7-S1 FJC $\widehat{E_1}$ strain magnitudes were significantly greater when the HLVA-SM was applied to the L7 vertebra compared with at the L5 vertebra (post-hoc Tukey test, $p < 0.05$). On the right side of the spine, L7-S1 FJC $\widehat{E_1}$ strain magnitudes did not differ significantly with manipulation site (post-hoc Tukey test, $p > 0.05$, power 62%).

3.4 FJC Minimum Principal Strain- $\widehat{E_2}$

During simulated HVLA-SM in the cat, regional $\widehat{E_2}$ FJC strain magnitudes varied with site-specific manipulation (Fig. 7; bottom). The effects of manipulation site and side of the spine on cat $\widehat{E_2}$ FJC strain magnitude varied depending on the joint level that was considered (i.e., L5–6, L6–7, or L7-S1).

Cat L5–6 $\widehat{E_2}$ FJC minimum principal strain magnitudes were significantly affected by manipulation site and side of the spine, and there were significant interactions between these two factors (two-way ANOVA; $p = 0.001$). L5–6 cat $\widehat{E_2}$ FJC principal strain magnitudes on the left side of the spine were greater in absolute magnitude when the HVLA-SM was applied to the L6 vertebra compared with the L7 vertebra (post-hoc Tukey test, $p < 0.05$). No significant difference was detected in L5–6 cat $\widehat{E_2}$ FJC principal strain magnitudes on the left side of the spine for other manipulation sites nor were significant differences detected in cat $\widehat{E_2}$ FJC principal strain magnitudes on the right side of the spine with varying HVLA-SM locations (post-hoc Tukey test, $p > 0.05$, power 66%).

At L6–7 and L7-S1, there were no significant associations detected between cat $\widehat{E_2}$ FJC principal strain magnitudes with HVLA-SM site or side of the spine (ANOVA, $p > 0.2$). Statistical power was less than 50%. This was due to the high variability in the data, which could have precluded detection of significant differences.

3.5 Regression Relationship Between Cat and Human FJC Principal Strain Magnitudes

Cat $\widehat{E_1}$ FJC strain magnitudes from the current study and human $\widehat{E_1}$ FJC strain magnitudes from a prior study [6] were compared quantitatively by developing regression relationships that expressed $\widehat{E_1}$ FJC strain magnitudes for a given FJC as a function of species, HVLA-SM site or interactions thereof. The coefficients for the regression relationships are depicted in Table 1. On the left side of the spine, $\widehat{E_1}$ FJC strain magnitudes in response to HVLA-SM were significant ($p < 0.05$) or approached significance ($p = 0.07$) and were moderately correlated ($R^2 > 0.45$). On the right side of the spine, $\widehat{E_1}$ FJC strain magnitudes did not demonstrate significant correlations during HVLA-SM, except at the cephalic and caudal joints where species was a significant predictor of $\widehat{E_1}$ strain ($p < 0.02$). $\widehat{E_1}$ FJC strain relationships on the right side of the spine were not well correlated ($R^2 < 0.4$).

4 Discussion

This is the first report of cat lumbar FJC strain magnitudes during simulated HVLA-SM. Similar to humans, site-specific HVLA-SM produced regional biomechanical effects producing substantial joint motion and FJC strain magnitudes over at least two segments from the manipulation site. Despite SM displacements being delivered along the *x*-axis (transverse), RVT occurred primarily along the spine's *y*-axis (cranial-caudal). RVT magnitudes were significantly affected by manipulation site at all joint levels. In the cat, IVA during HVLA-SM occurred primarily about the *z*-axis (dorsal-ventral) at L5–6, about the *z*- and *y*-axes at L7-S1, and were more complex at L6–7, regardless of manipulation site. FJC strain magnitude varied depending on the joint level and side of the spine relative to the manipulation site. At corresponding joint levels, FJC strain was larger in cats compared with humans. Significant regression relationships for cat and human lumbar spines were established using a general linear model, where species, HVLA-SM site, and interactions thereof were used to predict strain with moderate correlation. The relationships established in the current study can be used in future neurophysiological studies conducted in cats to extrapolate how human FJC afferents might respond to similar HVLA-SM.

Similar to prior in situ studies using human cadaveric lumbar spine specimens [6], this study reported vertebral motions during HVLA-SM in cat spine specimens and reported motions for all six possible degrees-of-freedom. Optically tracking these vertebral motions using six degrees-of-freedom overcame limitations associated with other methods of tracking vertebral motion in human studies. For instance, the kinematic system had higher temporal resolution compared with imaging modalities such as MRI [24,25] or X-ray [26]. The six

degrees–of-freedom measurements in the current study included rotation and translation data that would have been missed if 2D measurements were taken (as in Refs. [27–29]). This provided more precise information, eliminating errors due to out-of-plane motion. The measurement system differentiated between linear and angular motions unlike in prior studies that used accelerations to compute vertebral motions [30–32], which can overestimate vertebral movements [27].

IVA magnitudes during HVLA-SM in the cat were "biomechanically safe" when considering the magnitude of IVA physiological motions in vivo [33] and in situ [15]. The largest *z*-axis IVA magnitudes in the current study were similar to those measured during maximum extension-flexion in vivo [33] (i.e., 2.4 ± 1.8 deg versus ~7 deg at L5–6, 3.0 ± 2.7 deg versus ~2 deg at L6–7 and 2.0 ± 2.1 deg versus ~7.5 deg at L7-S1, respectively). In the current study, *x*-axis IVA was larger during simulated HVLA-SM compared with maximum physiological lateral bending in vivo [33] (i.e., 4.1 ± 2.0 deg versus ~3 deg at L5–6; 4.0 ± 2.8 deg versus ~2 at L6–7; 4.6 ± 3.1 deg versus near zero at L7-S1). The smaller lumbar IVAs measured in the in vivo study [33] may be attributable to differences in positioning of the animals, where flexibility in lateral bending was variable and likely dependent on rotation about the *y*-axis (torsion) in Ref. [33]. The results of the current study support this idea, particularly at L7-S1, where large *x*-axis rotations were associated with correspondingly large *y*-axis IVA. All IVA magnitudes during simulated HVLA-SM were well within the range measured during physiological motions using cat lumbar spine specimens measured a prior in situ study [15], again supporting the conclusion that HVLA-SM is biomechanically safe.

Joint motion (i.e., RVT and IVA) in cats was larger in magnitude compared with humans [6]. This was not surprising, as cat lumbar spines visually appear more flexible than humans [34] enabling them to gallop (flexion-extension) and groom (axial rotation/lateral bending), etc. [33]. Much of the motion in the lumbar region for humans occurs at the hips (i.e., flexion). FJC strain magnitudes during similar joint motions were also larger in cats compared with humans [6] suggesting that the FJC is less stiff in cats compared with humans. The macromolecular structures of cat and human FJC ligaments support this as cat lumbar spinal ligaments have higher elastin: collagen ratios [35] while human FJCs are comprised of highly organized collagen fibers (medial-lateral orientation) [36]. However, the human spine specimens used in the current study may have been excessively stiff having been obtained from an aged population while the cat spine specimens were from animals representing a younger age group.

The regression relationship developed in this study will allow extrapolation of neurophysiological data from cats to estimate how human FJC neurons might respond to biomechanically similar motions. If the joint level of interest and manipulation site is known for human, one can use the regression relationship to estimate the magnitude of resultant human FJC strain. Changing the dummy variable for species (i.e., *Sp*) in the regression relationship from human to cat will estimate the corresponding magnitude of strain for cat lumbar spines. The direction of the HVLA-SM affects the magnitude of strain that develops in a given FJC (as demonstrated as the side of spine in the current study). One can also consider parameters such as cat paraspinal afferent threshold, firing rate, and saturation as a function of FJC strain to predict how human afferents might respond to strains produced during clinically delivered HVLA-SM.

Cat FJC principal strain magnitudes were within the range measured during maximum in situ physiological motions (see Ref. [15]). Similar to the conclusion using human spine specimens [6], this implied that the "biomechanically safe" stimulus produced by an HVLA-SM was likely subthreshold for FJC mechanonociceptors. However, in the cervical spine,

subfailure FJC strain magnitudes were thought to cause microscopic damage and/or produce pain symptoms [37]. Correlating the findings of the current study to future neurophysiological studies in cats will provide additional evidence regarding the safety of HVLA-SM loading.

Similar to prior human in situ study [6], specific segmental HVLA-SM produced substantial intervertebral motions. In addition, FJC strain magnitudes occurred at least two segments from the manipulation site. In a prior clinical study of SM applied to the cervical spine, patients who received SM at a targeted motion segment selected because of clinical findings, experienced the same beneficial results as those who received SM at a targeted motion segment unrelated to the clinical findings [38]. This indicated that site-specific HVLA-SM may not be as important as previously postulated [38,39]. The current study demonstrated that the cat spine can be used as an appropriate model for investigating local versus regional effects during HVLA-SM. The procedure produced FJC strain magnitudes that could be sufficient to stimulate FJC neurons not only locally but several segments from the site of HVLA-SM application.

There are a number of limitations that should be considered when interpreting the results of this study. First, the applicability of the biomechanical model to neurophysiological questions is contingent on human and cat FJC afferents responding similarly. This assumption cannot be tested, as techniques that are employed to measure single-neuron responses are terminal and invasive; it would be unethical to conduct such experiments in humans. However in nonspinal tissues, mechanical thresholds are similar for low-threshold knee joint afferents in nonhuman primate [40] and cat [41–43], as are thresholds for low-threshold cutaneous afferents in human [44–46] and nonhuman primate [47–49], and cat [50,51]. A second consideration is that the cadaveric model used in the current study did not include superficial muscles, whose passive tension may alter FJC strain magnitudes in vivo. Paraspinal muscle contractions stiffen the spine, which could potentially decrease intervertebral motions during in vivo SM, decreasing FJC strains. Conversely, contraction of multifidi muscles, which have insertions on the FJC surface, could generate additional strain [52]. The muscle reflex response during HVLA SM in humans in vivo is delayed by 50–200 ms after the application of the thrust [53], whereas FJC strain magnitudes were measured at peak impulse in the current study. The muscle reflex could lead to additional sensory input from the FJC capsule if the strains it produced reached the FJC afferents' mechanical threshold.

In conclusion, regression relationships were established to relate cat and human FJC biomechanics during simulated HVLA-SM. The regression model was developed and validated using statistical analyses. The data obtained in the current study opens new avenues of investigation for resolving physiological mechanisms of HVLA-SM. Future work should include the investigation of the clinical relevance of site-specific manipulations in managing patients with low back pain given the apparent biomechanical safety of the procedure. Additional studies should also include investigation of FJC afferent single-neuron responses and population responses during different types of HVLA-SM.

Acknowledgments

This study was supported by funds from the National Institutes of Health National Center for Complementary and Alternative Medicine (Contract No. U19AT001701) and the Ruth L. Kirschstein National Research Service Award (Contract No. F31AT002666).

Nomenclature

$\mathbf{c_i}$	coefficients in the general linear model
$\widehat{E_1}$	= maximum prinicipal strain
$\widehat{E_2}$	= minimum prinicipal strain
L	dummy variable in the general linear model for manipulation site (level)
S	dummy variable in the general linear model for side of the spine
Sp	dummy variable in the general linear model for species

References

1. Wolsko PM, Eisenberg DM, Davis RB, Kessler R, Phillips RS. Patterns and Perceptions of Care for Treatment of Back and Neck Pain: Results of a National Survey. Spine. 2003; 28(3):292–297. [PubMed: 12567035]
2. Bronfort G. Spinal Manipulation: Current State of Research and Its Indications. Neurol Clin. 1999; 17(1):91–111. [PubMed: 9855673]
3. Bronfort G, Haas M, Evans RL, Bouter LM. Efficacy of Spinal Manipulation and Mobilization for Low Back Pain and Neck Pain: A Systematic Review and Best Evidence Synthesis. Eur Spine J. 2004; 4(3):335–356.
4. Triano, J.; Herzog, W. Clinical Biomechanics of Spinal Manipulation. Churchill Livingstone; New York: 2000. The Mechanics of Spinal Manipulation; p. 92-190.
5. Shekelle PG, Markovich M, Louie R. Factors Associated With Choosing a Chiropractor for Episodes of Back Pain Care. Med Care. 1995; 33(8):842–850. [PubMed: 7637405]
6. Ianuzzi A, Khalsa PS. Comparison of Human Lumbar Facet Joint Capsule Strains During Simulated High-Velocity, Low-Amplitude Spinal Manipulation Versus Physiological Motions. Eur Spine J. 2005; 5(3):277–290.
7. Ianuzzi A, Khalsa PS. High Loading Rate During Spinal Manipulation Produces Unique Facet Joint Capsule Strain Patterns Compared With Axial Rotations. J Manipulative Physiol Ther. 2005; 28(9): 673–687. [PubMed: 16326237]
8. Triano J, Schultz AB. Loads Transmitted During Lumbosacral Spinal Manipulative Therapy. Spine. 1997; 22(17):1955–1964. [PubMed: 9306523]
9. Pickar JG, Kang YM. Paraspinal Muscle Spindle Responses to the Duration of a Spinal Manipulation Under Force Control. J Manipulative Physiol Ther. 2006; 29(1):22–31. [PubMed: 16396726]
10. Pickar JG, Sung PS, Kang YM, Ge W. Response of Lumbar Paraspinal Muscles Spindles is Greater to Spinal Manipulative Loading Compared With Slower Loading Under Length Control. Eur Spine J. 2007; 7(5):583–595.
11. Cavanaugh JM, Ozaktay AC, Yamashita HT, King AI. Lumbar Facet Pain: Biomechanics, Neuroanatomy and Neurophysiology. J Biomech. 1996; 29(9):1117–1129. [PubMed: 8872268]
12. Cavanaugh JM, Ozaktay AC, Yamashita T, Avramov A, Getchell TV, King AI. Mechanisms of Low Back Pain: A Neurophysiologic and Neuroanatomic Study. Clin Orthop Relat Res. 1997; 335:166–180. [PubMed: 9020216]
13. McLain RF, Pickar JG. Mechanoreceptor Endings in Human Thoracic and Lumbar Facet Joints. Spine. 1998; 23(2):168–173. [PubMed: 9474721]
14. Pickar JG. Neurophysiological Effects of Spinal Manipulation. Eur Spine J. 2002; 2(5):357–371.
15. Ianuzzi A, Pickar JG, Khalsa PS. Validation of the Cat as a Model for the Human Lumbar Spine During Physiological Motions. 2009 submitted.
16. Bogduk N. The Dorsal Lumbar Muscles of the Cat. Anat Anz. 1980; 148(1):55–67. [PubMed: 7212283]
17. Pickar JG, McLain RF. Responses of Mechanosensitive Afferents to Manipulation of the Lumbar Facet in the Cat. Spine. 1995; 20(22):2379–2385. [PubMed: 8578387]

18. Ianuzzi A, Little JS, Chiu JB, Baitner A, Kawchuk G, Khalsa PS. Human Lumbar Facet Joint Capsule Strains: I. During Physiological Motions. Eur Spine J. 2004; 4(2):141–152.
19. Pickar JG, Wheeler JD. Response of Muscle Proprioceptors to Spinal Manipulative-Like Loads in the Anesthetized Cat. J Manipulative Physiol Ther. 2001; 24(1):2–11. [PubMed: 11174689]
20. Söderkvist I, Wedin PA. Determining the Movements of the Skeleton Using Well-Configured Markers. J Biomech. 1993; 26(12):1473–1477. [PubMed: 8308052]
21. Gaudette GR, Todaro J, Krukenkamp IB, Chiang FP. Computer Aided Speckle Interferometry: A Technique for Measuring Deformation of the Surface of the Heart. Ann Biomed Eng. 2001; 29(9): 775–780. [PubMed: 11599585]
22. Hatze H. High-Precision Three-Dimensional Photogrammetric Calibration and Object Space Reconstruction Using a Modified DLT-Approach. J Biomech. 1988; 21(7):533–538. [PubMed: 3410856]
23. Winkelstein BA, Nightingale RW, Richardson WJ, Myers BS. The Cervical Facet Capsule and Its Role in Whiplash Injury: A Biomechanical Investigation. Spine. 2000; 25(10):1238–1246. [PubMed: 10806500]
24. Cramer GD, Gregerson DM, Knudsen JT, Hubbard BB, Ustas LM, Cantu JA. The Effects of Side-Posture Positioning and Spinal Adjusting on the Lumbar Z Joints: A Randomized Controlled Trial With Sixty-Four Subjects. Spine. 2002; 27(22):2459–2466. [PubMed: 12435975]
25. Pearcy MJ, Bogduk N. Instantaneous Axes of Rotation of the Lumbar Intervertebral Joints. Spine. 1988; 13(9):1033–1041. [PubMed: 3206297]
26. Lee R, Evans J. An In Vivo Study of the Intervertebral Movements Produced by Posteroanterior Mobilization. Clin Biomech (Bristol, Avon). 1997; 12(6):400–408.
27. Gal J, Herzog W, Kawchuk G, Conway P, Zhang YT. Measurements of Vertebral Translations Using Bone Pins, Surface Markers and Accelerometers. Clin Biomech (Bristol, Avon). 1997; 12(5):337–340.
28. Gal J, Herzog W, Kawchuk G, Conway PJ, Zhang YT. Movements of Vertebrae During Manipulative Thrusts to Unembalmed Human Cadavers. J Manipulative Physiol Ther. 1997; 20(1):30–40. [PubMed: 9004120]
29. Gal JM, Herzog W, Kawchuk GN, Conway PJ, Zhang YT. Forces and Relative Vertebral Movements During SMT to Unembalmed Post-Rigor Human Cadavers: Peculiarities Associated With Joint Cavitation. J Manipulative Physiol Ther. 1995; 18(1):4–9. [PubMed: 7706960]
30. Cohen E, Triano JJ, McGregor M, Papakyriakou M. Biomechanical Performance of Spinal Manipulation Therapy by Newly Trained vs. Practicing Providers: Does Experience Transfer To Unfamiliar Procedures? J Manipulative Physiol Ther. 1995; 18(6):347–352. [PubMed: 7595108]
31. Keller TS, Colloca CJ, Gunzburg R. Neuromechanical Characterization of In Vivo Lumbar Spinal Manipulation. Part I. Vertebral Motion. J Manipulative Physiol Ther. 2003; 26(9):567–578. [PubMed: 14673406]
32. Maigne JY, Guillon F. Highlighting of Intervertebral Movements and Variations of Intradiskal Pressure During Lumbar Spine Manipulation: A Feasibility Study. J Manipulative Physiol Ther. 2000; 23(8):531–535. [PubMed: 11050609]
33. Macpherson JM, Ye Y. The Cat Vertebral Column: Stance Configuration and Range of Motion. Exp Brain Res. 1998; 119(3):324–332. [PubMed: 9551833]
34. Ianuzzi A, Pickar JG, Khalsa PS. Determination of Torque-Limits for Human and Cat Lumbar Spine Specimens During Displacement-Controlled Physiological Motions. Spine J. 2009; 9(1):77–86. [PubMed: 17983845]
35. Heylings DJ. Supraspinous and Interspinous Ligaments in Dog, Cat and Baboon. J Anat. 1980; 130(Pt 2):223–228. [PubMed: 6772620]
36. Yamashita T, Minaki Y, Ozaktay AC, Cavanaugh JM, King AI. A Morphological Study of the Fibrous Capsule of the Human Lumbar Facet Joint. Spine. 1996; 21(5):538–543. [PubMed: 8852306]
37. Lee KE, Franklin AN, Davis MB, Winkelstein BA. Tensile Cervical Facet Capsule Ligament Mechanics: Failure and Subfailure Responses in the Rat. J Biomech. 2005; 39(7):1256–1264. [PubMed: 15899488]

38. Haas M, Groupp E, Panzer D, Partna L, Lumsden S, Aickin M. Efficacy Of Cervical Endplay Assessment as an Indicator for Spinal Manipulation. Spine. 2003; 28(11):1091–1096. [PubMed: 12782973]
39. Jull G, Bogduk N, Marsland A. The Accuracy of Manual Diagnosis for Cervical Zygapophysial Joint Pain Syndromes. Med J Aust. 1988; 148(5):233–236. [PubMed: 3343953]
40. Grigg P, Greenspan BJ. Response of Primate Joint Afferent Neurons to Mechanical Stimulation of Knee Joint. J Neurophysiol. 1977; 40(1):1–8. [PubMed: 401873]
41. Burgess PR, Clark FJ. Characteristics of Knee Joint Receptors in the Cat. J Physiol (London). 1969; 203(2):317–335. [PubMed: 5796466]
42. Grigg P. Mechanical Factors Influencing Response of Joint Afferent Neurons From Cat Knee. J Neurophysiol. 1975; 38(6):1473–1484. [PubMed: 1221084]
43. Khalsa PS, Grigg P. Responses of Mechanoreceptor Neurons in the Cat Knee Joint Capsule Before and After Anterior Cruciate Ligament Transection. J Orthop Res. 1996; 14(1):114–122. [PubMed: 8618153]
44. Vallbo AB, Hagbarth KE. Activity From Skin Mechanoreceptors Recorded Percutaneously in Awake Human Subjects. Exp Neurol. 1968; 21(3):270–289. [PubMed: 5673644]
45. Vallbo AB, Olausson H, Wessberg J, Kakuda N. Receptive Field Characteristics of Tactile Units With Myelinated Afferents in Hairy Skin of Human Subjects. J Physiol (London). 1995; 483(3): 783–795. [PubMed: 7776258]
46. Edin B. Cutaneous Afferents Provide Information About Knee Joint Movements in Humans. J Physiol (London). 2001; 531(1):289–297. [PubMed: 11179411]
47. Freeman AW, Johnson KO. Cutaneous Mechanoreceptors in Macaque Monkey: Temporal Discharge Patterns Evoked by Vibration, and a Receptor Model. J Physiol (London). 1982; 323:21–41. [PubMed: 7097573]
48. Mountcastle VB, LaMotte RH, Carli G. Detection Thresholds for Stimuli in Humans and Monkeys: Comparison With Threshold Events in Mechanoreceptive Afferent Nerve Fibers Innervating the Monkey Hand. J Neurophysiol. 1972; 35(1):122–136. [PubMed: 4621505]
49. Khalsa PS, Friedman RM, Srinivasan MA, Lamotte RH. Encoding of Shape and Orientation of Objects Indented Into the Monkey Fingerpad by Populations of Slowly and Rapidly Adapting Mechanoreceptors. J Neurophysiol. 1998; 79(6):3238–3251. [PubMed: 9636122]
50. Iggo A, Muir AR. The Structure and Function of a Slowly Adapting Touch Corpuscle in Hairy Skin. J Physiol (London). 1969; 200(3):763–796. [PubMed: 4974746]
51. Horch KW, Burgess PR. Effect of Activation and Adaptation on the Sensitivity of Slowly Adapting Cutaneous Mechanoreceptors. Brain Res. 1975; 98(1):109–118. [PubMed: 1175054]
52. Little JS, Ianuzzi A, Chiu JB, Baitner A, Khalsa PS. Human Lumbar Facet Joint Capsule Strains: II. Alteration of Strains Subsequent to Anterior Interbody Fixation. Eur Spine J. 2004; 4(2):153–162.
53. Herzog W, Scheele D, Conway PJ. Electromyographic Responses of Back and Limb Muscles Associated With Spinal Manipulative Therapy. Spine. 1999; 24(2):146–152. [PubMed: 9926385]

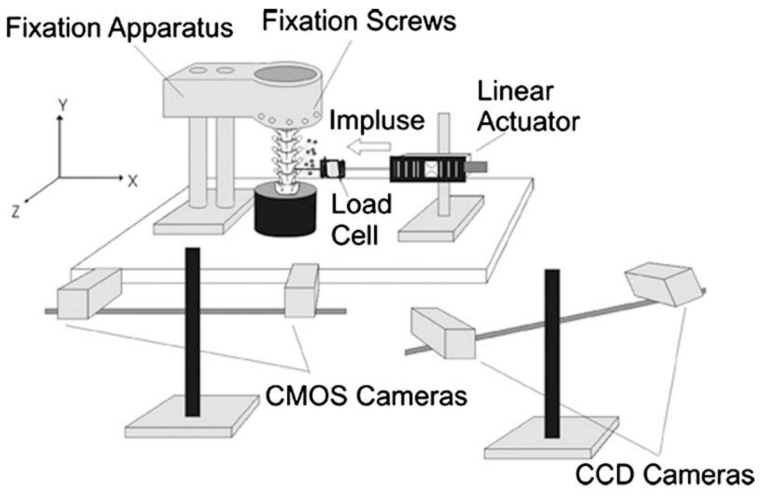

Fig. 1.

Experimental setup for simulated spinal manipulation using a cat lumbar spine specimen. Specimens were fixed in the neutral posture using the spine fixation apparatus. A linear actuator was coupled to the L5, L6, or L7 vertebral body and actuated in the direction shown. The load cell measured the developed force. CCD cameras optically tracked markers attached to L5–L7 transverse processes for kinematic measurements and CMOS cameras were used for optically measuring facet joint capsule strain.

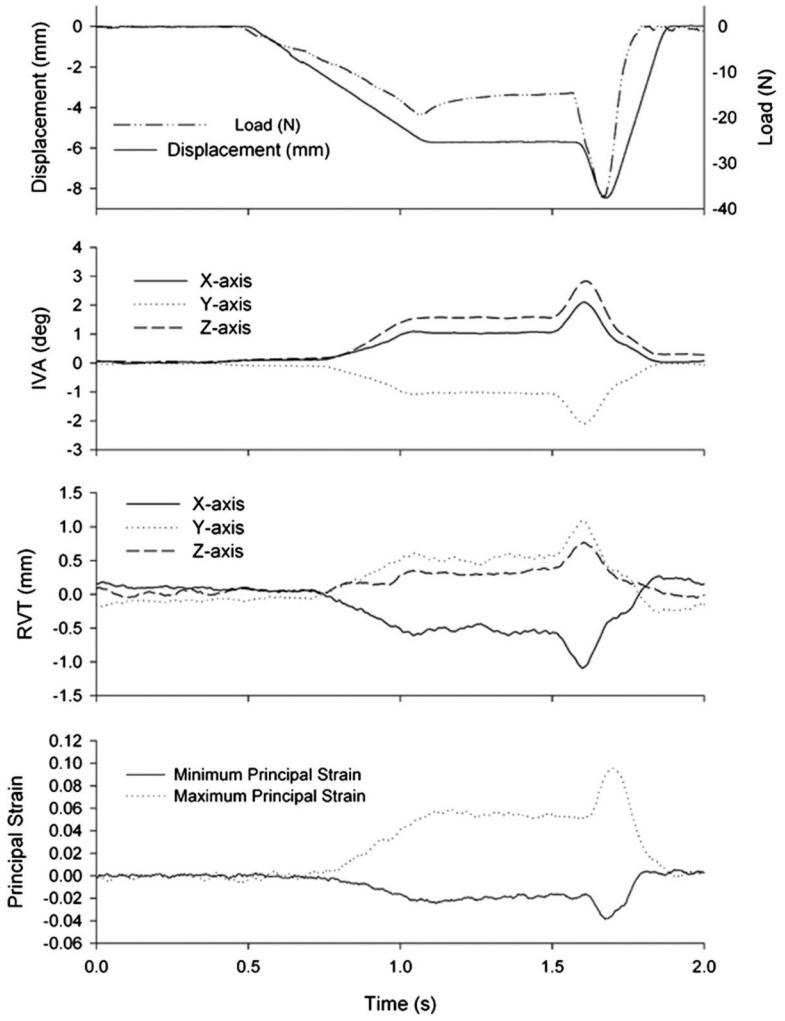

Fig. 2.

Representative data from simulated spinal manipulation applied to L6. Displacement was the controlled parameter. Developed force, IVA, RVT, and facet joint capsule principal strain magnitudes (L6–7 shown) were measured simultaneously. Note that displacements were applied in the *x*-direction and the negative force values indicate loading in the same direction.

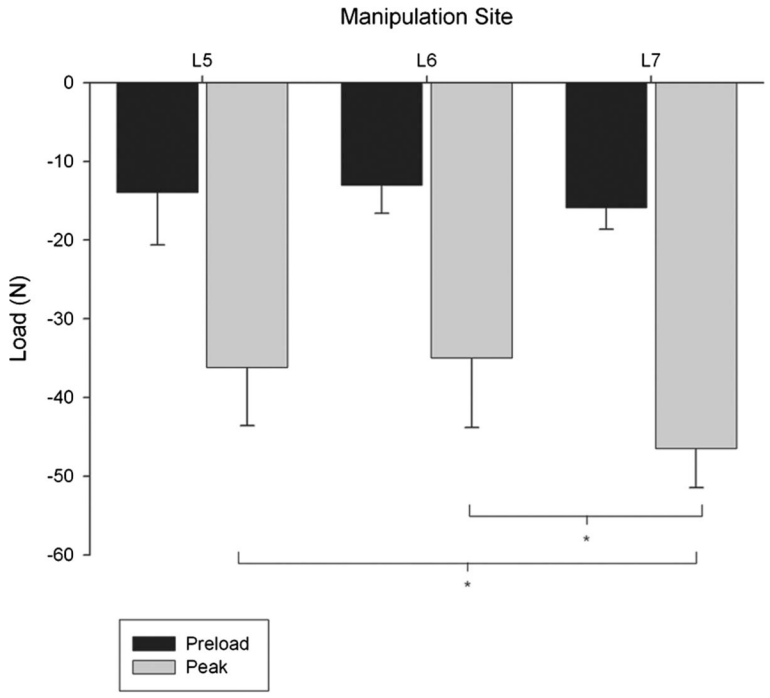

Fig. 3.

Developed load during simulated manipulation for cat lumbar spine specimens during the preload and peak impulse. Peak force with constant total vertebral displacement was significantly greater when the manipulation was applied to L7 compared with L5 and L6 (one-way analysis of variance with post-hoc Student–Newman–Keuls test; $p < 0.05$). Error bars show standard deviations.

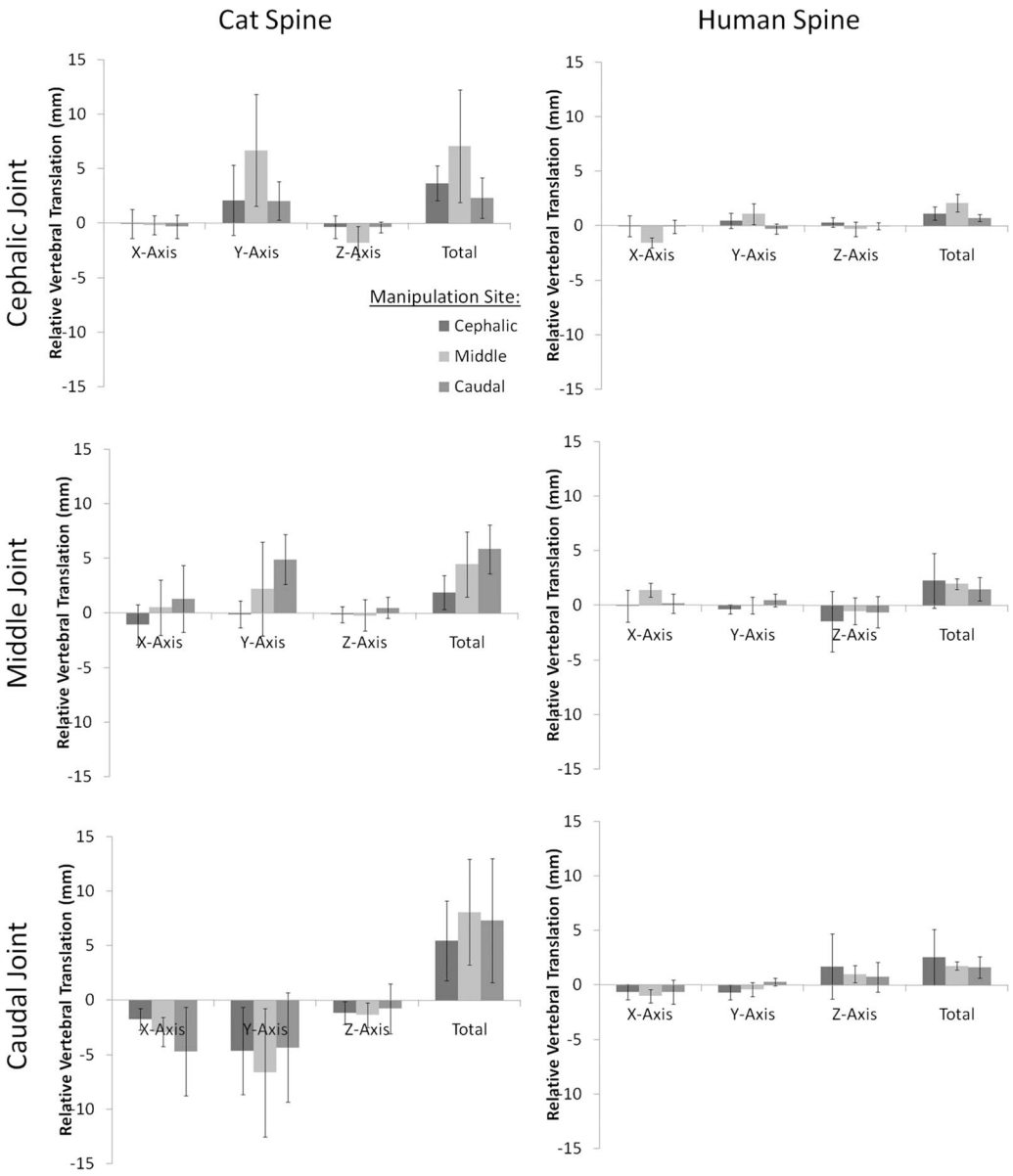

Fig. 4.

RVT during simulated spinal manipulation in cat and human lumbar spine specimens. Error bars show standard deviations.

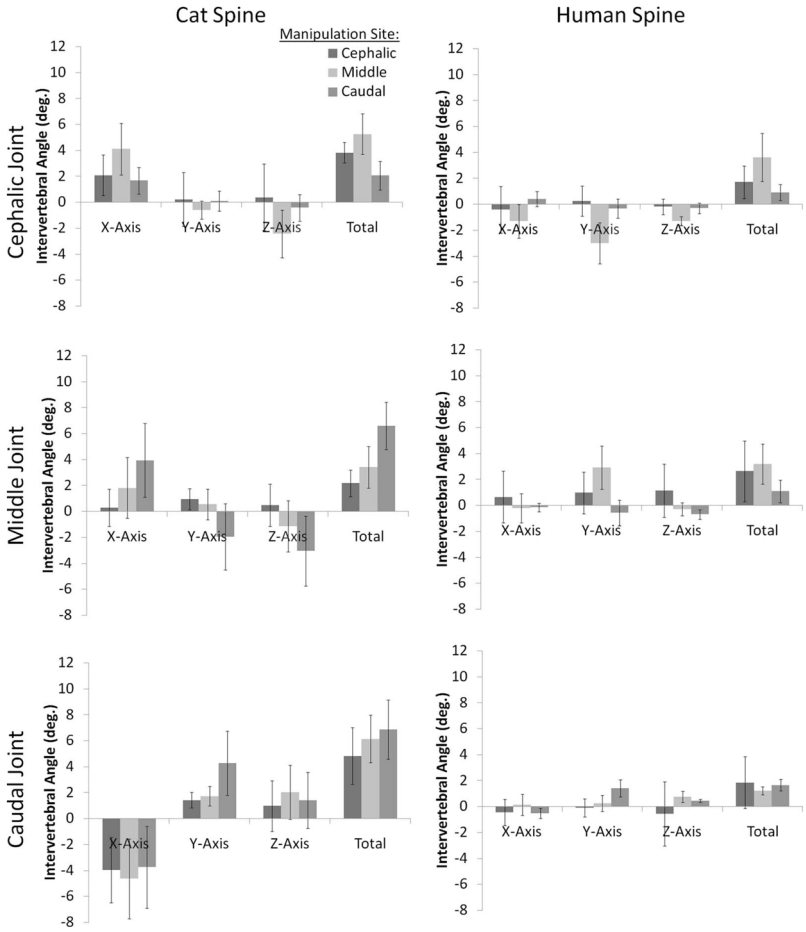

Fig. 5.
IVA during simulated spinal manipulation using cat and human lumbar spine specimens. Error bars show standard deviations.

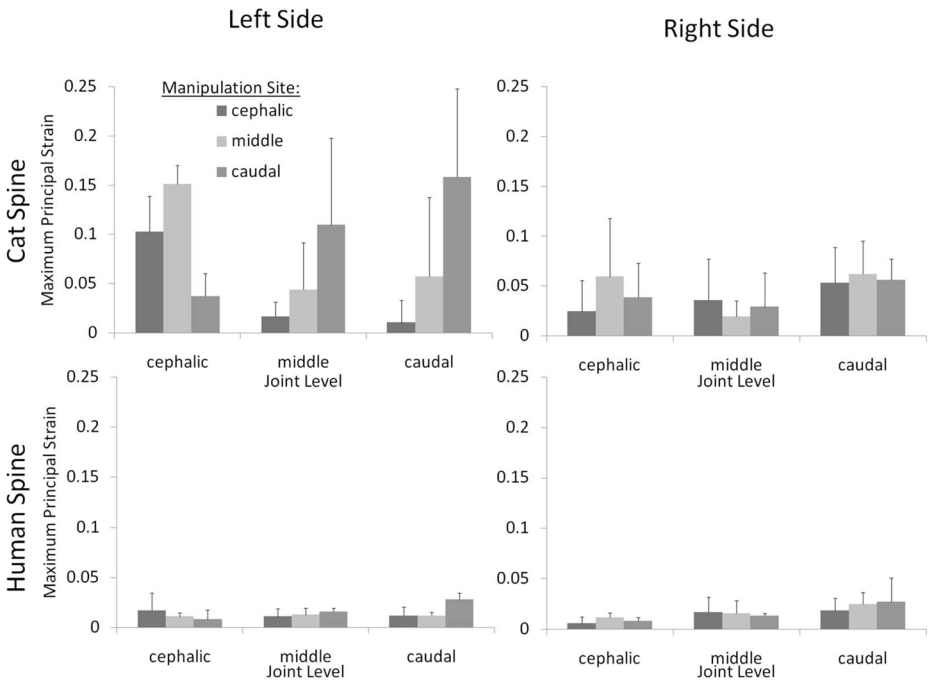

Fig. 6.

Cat lumbar facet joint capsule strain magnitudes during simulated manipulation applied at L5, L6, or L7. Manipulations were delivered at the manipulation site indicted by applying a simultaneous translation (right to left) and rotation (counterclockwise) of the vertebrae. Error bars show standard deviations.

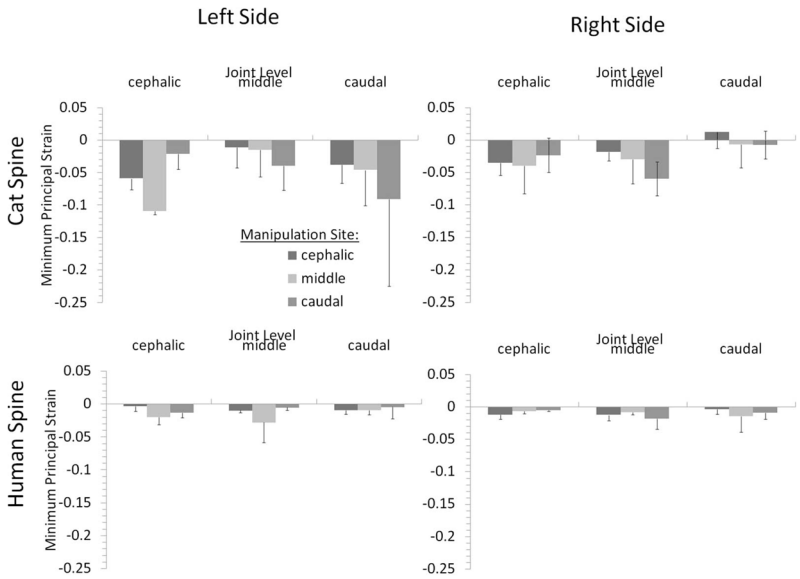

Fig. 7.

Human lumbar facet joint capsule strain magnitudes during simulated spinal manipulation applied to the anterior aspect of L3, L4, or L5. Manipulations were delivered by applying a simultaneous translation (right to left) and rotation (counterclockwise) of the manipulated vertebra. Error bars show standard deviations.

Table 1

Coefficients for the regression model comparing can and human $\widehat{E_1}$ FJC strain magnitudes as functions of species (cat versus human) and HVLA-SM site (cephalic, middle, or caudal vertebra). The coefficients fit the following equation: $\widehat{E_1}=c_0+c_1Sp+\mathrm{Loc}_1+\mathrm{Loc}_2Sp$, where c_0 is a constant, $Sp = +1$ for cat and $Sp = -1$ for human spines, and Loc_1 and Loc_2 vary with HVLA-SM site as specified in the table below.

			Cephalic HVLA-SM		Middle HVLA-SM		Caudal HVLA-SM	
FJC	c_0	c_1	Loc_1	Loc_2	Loc_1	Loc_2	Loc_1	Loc_2
Left cephalic	0.055	0.043	0.005	0.000	0.026	0.028	−0.032	−0.028
Left middle	0.035	0.022	−0.021	−0.019	−0.007	−0.006	0.028	0.025
Left caudal	0.046	0.029	−0.035	−0.030	−0.012	−0.006	0.047	0.036
Right cephalic	0.025	0.016	−0.009	−0.007	0.011	0.008	−0.001	−0.001
Right middle	0.022	0.006	0.005	0.003	−0.004	−0.004	0.000	0.001
Right caudal	0.040	0.017	−0.004	0.001	0.003	0.002	0.001	−0.002